Bioactive Materials 17 (2022) 234–247

Contents lists available at ScienceDirect

Bioactive Materials

journal homepage: www.keaipublishing.com/en/journals/bioactive-materials

3D printed biomimetic epithelium/stroma bilayer hydrogel implant for corneal regeneration

Binbin He [a], Jie Wang [b], Mengtian Xie [a], Miaoyi Xu [a], Yahan Zhang [a], Huijie Hao [c], Xiaoli Xing [c], William Lu [d], Quanhong Han [b,**], Wenguang Liu [a,*]

[a] School of Material Science and Engineering, Tianjin Key Laboratory of Composite and Functional Materials, Tianjin University, Tianjin, 300350, China
[b] Clinical College of Ophthalmology, Tianjin Medical University, Tianjin Key Lab of Ophthalmology and Visual Science, Tianjin Eye Institute, Tianjin Eye Hospital, Gansu Road 4, Heping District, Tianjin, 300020, China
[c] Tianjin International Joint Research and Development Centre of Ophthalmology and Vision Science, Eye Institute and School of Optometry, Tianjin Medical University Eye Hospital, Tianjin, 300384, China
[d] Department of Orthopaedic and Traumotology, The University of Hong Kong, 21 Sassoon Rd, Hong Kong, PR China

ARTICLE INFO

Keywords:
3D printing
Hydrogel
Bi-layer scaffold
Corneal regeneration

ABSTRACT

Corneal regeneration has always been a challenge due to its sophisticated structure and undesirable keratocyte-fibroblast transformation. Herein, we propose 3D printing of a biomimetic epithelium/stroma bilayer implant for corneal regeneration. Gelatin methacrylate (GelMA) and long-chain poly(ethylene glycol) diacrylate (PEGDA) are blended to form a two-component ink, which can be printed to different mechanically robust programmed PEGDA-GelMA objects by Digital Light Processing (DLP) printing technology, due to the toughening effect of crystalline crosslinks from long-chain PEGDA on GelMA hydrogel after photo-initiated copolymerization. The printed PEGDA-GelMA hydrogels support cell adhesion, proliferation, migration, meanwhile demonstrating a high light transmittance, and an appropriate swelling degree, nutrient permeation and degradation rate. A bi-layer dome-shaped corneal scaffold consisting of rabbit corneal epithelial cells (rCECs)-laden epithelia layer and rabbit adipose-derived mesenchymal stem cells (rASCs)-laden orthogonally aligned fibrous stroma layer can be printed out with a high fidelity and robustly surgical handling ability. This bi-layer cells-laden corneal scaffold is applied in a rabbit keratoplasty model. The post-operative outcome reveals efficient sealing of corneal defects, re-epithelialization and stromal regeneration. The concerted effects of microstructure of 3D printed corneal scaffold and precisely located cells in epithelia and stroma layer provide an optimal topographical and biological microenvironment for corneal regeneration.

1. Introduction

Cornea is a transparent, dome-shaped tissue covering the front of the eye, which protects the intraocular structures from the external environment, and plays a crucial role in light transmittance and refraction [1]. It consists of three main layers (i.e., the epithelium, stroma, and endothelium), among which corneal stroma constitutes 90% of the whole thickness. Stroma comprised of orthogonally aligned collagen nanofibrous lamellae is critical for both the mechanical and optical property of the cornea [2]. When the cornea is damaged, a large quantity of irregularly deposited collagenous matrices are secreted, which leads to light scattering and corneal scarring, consequently causing visual impairment or even blindness [3]. It is estimated that over 10 million patients with diverse corneal diseases are reported annually [4]. Despite success of human donor corneal transplantation and effort to construct bioinert corneal substitutes for clinical applications, donor shortage, disease transmission, high rate of severe complications, and life-time immune suppression limit their applications. These materials are generally utilized only in end-stage injured corneas [5–7]. To address these concerns, a variety of bioengineering approaches have been proposed to develop corneal scaffolds based on decellularized cornea [8], amniotic membrane [9], natural (e.g., gelatin methacrylate (GelMA)

Peer review under responsibility of KeAi Communications Co., Ltd.
* Corresponding author.
** Corresponding author.
E-mail addresses: hanquanhong126@126.com (Q. Han), wgliu@tju.edu.cn (W. Liu).

https://doi.org/10.1016/j.bioactmat.2022.01.034
Received 7 December 2021; Received in revised form 11 January 2022; Accepted 17 January 2022
Available online 24 January 2022

[10,11], collagen [12–14], hyaluronate [15,16], alginate [17], etc) or synthetic (e.g., poly(ethylene glycol) (PEG) [18], poly(2-hydroxyethyl methacrylate) (PHEMA) [19], etc) polymers. Although these constructs have exhibited similar properties to the natural cornea, only a few of them could manage to reach Phase I of clinical trials due to the complicated fabrication procedure, low transparency, insufficient mechanical stability after application, and poor biointegration with tissues [20,21]. Currently, there is still no engineered corneal scaffold available for routine clinical use. Traditional fabrication of corneal scaffolds is casting. However, in this case, personalized molds with various parameters need to be customized due to distinct geometrical features of patient's cornea, which is time-consuming and costly [22]. Cornea has complex multi-layer structure and lamella are orthogonally aligned in its stroma. However, conventional fabrication methods frequently imitate only one layer of cornea and cannot realize the structural mimicry of native cornea.

3D bioprinting, the emerging technology that enables digital fabrication of cell-laden three-dimensional engineered constructs by layer-by-layer deposition of cells and biomaterials, offers a promising opportunity to customize individualized corneal scaffolds without resorting to molds [23–25]. In recent years, extrusion bioprinting has attracted significant attention to fabricating tissue engineering scaffolds [26,27]. However, to reach a high resolution, small nozzles (below 100 μm diameter) are required, which unavoidably impairs the cell viability due to highly shear stress-induced damage to the cells [28]. Besides, extrusion bioprinting is time-consuming and cannot meet the requirements of corneas for curvature and smooth surface [29,30]. Digital Light Processing (DLP), as one of the light-assisted 3D printing technologies, is based on a local photopolymerization of liquid photo-initiated curable ink layer by layer [31]. DLP is superior to extrusion printing in terms of high cell viability during printing process, high resolution (about 1 μm), and rapid printing speed [32]. Thus, DLP is promising to achieve precise spatial organization of different cells in the same tissue engineering scaffold, thus realizing the recapitulation of multi-layer structure of native cornea. Nonetheless, developing a bioink with an appropriate printing rheological property, high transparency, preserved cell viability and robust mechanical strength is the premise for successful construction of a tissue engineering corneal scaffold.

GelMA is one of the most widely used inks in 3D printing due to its photocrosslinkable property and good cell affinity [33]. However, the intrinsic brittleness of GelMA hydrogel limits its surgical handling. In this study, to develop a robust bioink for 3D printing corneal construct, we propose to design a two-component ink composed of GelMA and biocompatible long-chain poly(ethylene glycol) diacrylate (PEGDA) (Fig. 1A). The flexible PEGDA network is expected to toughen the GelMA hydrogel network owing to its energy dissipating mechanism (crystalline domain). The physicochemical properties of corneal scaffolds are systematically assessed through mechanical, rheological, optical, swelling and degradation tests. The cytocompatibility of hydrogel including cell adhesion, proliferation and migration is examined by using rabbit corneal epithelial cells (rCECs). To study the printability of hydrogels, bioink loading rCECs will be 3D printed by DLP technology

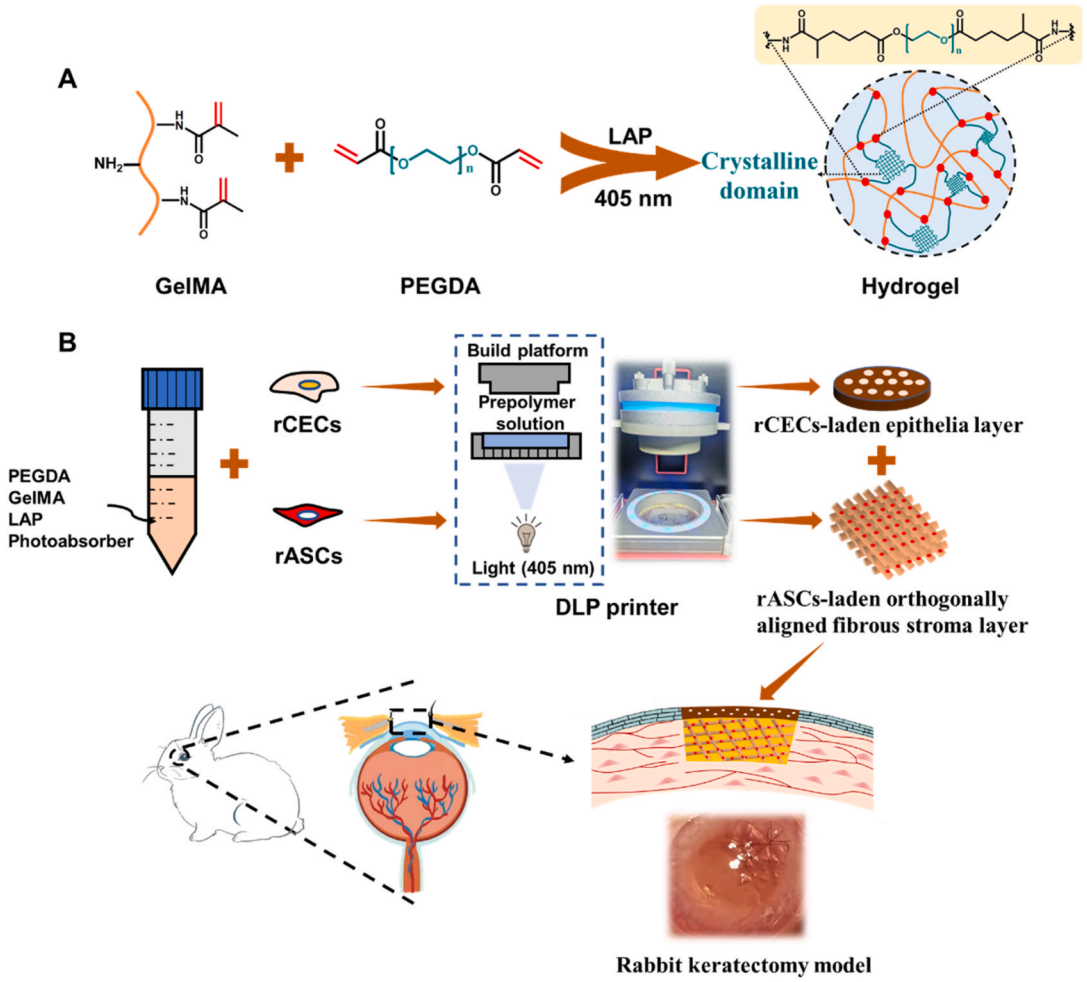

Fig. 1. (A) Components of ink and schematic illustration of network formation in PEGDA-GelMA hydrogel. (B) Description of the 3D bioprinting process and its application in a rabbit keratectomy model by using a bi-layer dome-shaped corneal scaffold consisting of rCECs-laden epithelia layer and rASCs-laden orthogonally aligned fibrous stroma layer.

into dome-shaped cornea and stroma-like orthogonally aligned fiber. In the animal study, a cell-laden bi-layer construct consisting of epithelium layer (loading rCECs) and orthogonally aligned fibrous stroma layer (loading rabbit adipose-derived mesenchymal stem cells (rASCs)) will be printed and used in a rabbit keratectomy model (Fig. 1B). Biocompatibility *in vivo* and corneal wound healing effects of hydrogels will be measured through ophthalmic and histopathological tests. To the best of our knowledge, very few studies have realized the corneal printing with curvature emulation by using DLP and precisely printed different source of cells in distinct layers to regenerate both the stroma and epithelium *in vivo*. Our results demonstrate that the synergistic effects of microstructure and precisely located cells can provide the most suitable topographical and biological environment for boosting corneal regeneration.

2. Materials and methods

2.1. Materials

Poly(ethylene glycol) (PEG, M_n = 8 kg/mol, 98%), type A porcine skin gelatin (300 bloom, 98%), type I collagenase (99%) were purchased from Sigma-Aldrich (Shanghai, China). Acryloyl chloride (97%), mechacrylic anhydride (97%) and triethylamine (99%) were obtained from Heowns Company (Tianjin, China). Photoinitiator lithium phenyl-2,4,6 trimethylbenzoyl phosphinate (LAP, 98%) and photoabsorber (orange food color, 98%) were purchased from EFL Company (Suzhou, China). L929 mouse fibroblast cells (L929), rabbit corneal epithelial cells (rCECs) and corresponding complete media were provided by BFB Company (Shanghai, China). Rabbit adipose-derived mesenchymal stem cells (rASCs) and complete medium were provided by Cyagen Company (Suzhou, China). Live/dead assay kit, 3-(4,5-dimethyl-2-thiazolyl)-2,5-diphenyl-2-H-tetrazolium bromide (MTT) and cell counting kit-8 (CCK-8) were obtained from Invitrogen Life Technologies (USA). All other chemicals and solvent were analytical reagents and used as received.

2.2. Synthesis of GelMA

GelMA was synthesized as previously described [34]. Briefly, 4 g gelatin was dissolved in 200 mL ultrapure water at 40 °C. Then, 132 mL dimethylformamide (DMF) was added to the solution. When a homogeneous solution was formed, 582 μL methacrylic anhydride was added in two steps and the reaction proceeded for 2 h at 40 °C. Then, the resulting solution was precipitated in ethanol twice and dissolved in ultrapure water at 37 °C. The product was obtained by lyophilization.

2.3. Synthesis of PEGDA

10 g PEG was dissolved in 50 mL dichloromethane, followed by the addition of 1 mL triethylamine. After cooling to 0 °C in an ice bath, 0.6 mL acryloyl chloride and 20 mL dichloromethane were added dropwise under stirring at 0 °C for about 1 h. Then the mixture was further stirred overnight at room temperature. After that, the mixture was precipitated with diethyl ether. The resultant PEGDA was obtained by filtration and drying in vacuo.

2.4. DLP 3D printing of hydrogels

The ink solution was prepared by mixing PEGDA + GelMA solution and photoinitator (LAP) + photoabsorber (orange food color) solution at 37 °C. All the materials were filtered by 0.22 μm membrane for sterilization. Then, PEGDA was dissolved in phosphate buffered saline (PBS) with 10, 15, 20 wt% concentrations. GelMA was dissolved in PBS at 37 °C with a 5 wt% concentration. Then, PEGDA and GelMA solutions were mixed together under an equal volume ratio. Subsequently, LAP and photoabsorber solutions were added to the PEGDA + GelMA mixture with a final concentration of 0.25 wt% and 0.05 wt%, respectively. The mixed solution was vortexed and incubated at 37 °C until clarification.

A DLP apparatus (BP8600, EFL Company, China) was used to print the desired hydrogels. The prepared ink solution was transferred into the ink box placed below the build platform, onto which the cured hydrogel could attach. After inputting pre-designed 3D models and printing parameters in computer (layer thickness and curing time), STereoLithography (STL) files were sliced programmatically in the Z direction and slices were projected for every layer to create the pre-designed 3D morphology. Printing was started by controlling the movement of ink box and images to the projector. The ink was exposed to blue light (405 nm, 10 mW/cm^2) during this process. When the printing was completed, the 3D constructed hydrogel was removed from the build platform and used for further measurement. Printing conditions were set as layer thickness of 50 μm and curing time of 20 s except for special instructions. The obtained hydrogel was named as PEGDA-GelMA-x-y, where x and y represented the initial polymer concentration of PEGDA and GelMA, respectively.

2.5. Characterizations

The chemical structures of PEG, PEGDA, gelatin, GelMA, and PEGDA-GelMA hydrogels were characterized by ^{1}H NMR spectra on a nuclear magnetic resonance (NMR) spectrometer (AVANCE III, 400 MHz, Bruker) using D_2O as the solvent. The methacylation degree (MD) of GelMA was defined as the ratio between the number of methacrylated groups attached to gelatin and the number of amine groups (lysine, hydroxylysine) of unreacted gelatin prior to the reaction [35]. The MD was calculated by:

$$MD = (1 - \frac{Lysine\ integration\ signal\ of\ GelMA}{Lysine\ integration\ signal\ of\ gelatin}) \times 100\% \quad (1)$$

Fourier transform infrared (FTIR) spectrometry (Nicolet 6700, ThermoFisher Scientific) was used to characterize the formation of PEGDA and GelMA. X-ray diffraction (XRD) patterns were collected by an X-ray diffractometer (D/Max2500, Rigaku) with a scanning speed of 5°/min and a scan range of 2θ from 4° to 40°. The equilibrium water contents (EWCs) of the hydrogels were measured by a gravimetric method [36]. The light transmittance of hydrogel was determined using a UV/vis spectrophotometer (GENESYS 180, ThermoFisher Scientific) over a wavelength range from 400 to 800 nm using PBS as a blank.

2.6. Measurement of mechanical properties

The mechanical properties of the hydrogels were tested on Instron 2344 Microtester at room temperature. Firstly, hydrogels were printed and immersed in PBS until swelling equilibrium. Then, dumbbell- (35 mm × 2 mm, GB/T 528 standard) or cylindrical- (5 mm × 5 mm) shaped hydrogels were used in tensile and compressive tests, respectively. The tensile strength, elongation at break and compressive strength were obtained directly from the stress-strain curves, and tensile and compressive modulus were derived from the slope of linear region (10%–20% strain) of the stress-strain curves. The tensile and compression rate were set at 10 mm/min. Six samples were tested per group.

2.7. Swelling and degradation behavior of hydrogels

Firstly, the samples were printed in a cylindrical (5 mm × 5 mm) shape. For swelling test, the hydrogels were immersed in PBS at 37 °C and weighed at the predetermined time to monitor the increased weight. The swelling degree (SD) of samples was calculated as follows:

$$SD = \frac{W_t - W_0}{W_0} \times 100\% \quad (2)$$

where W_t was the sample weight at different time points and W_0 was the initial weight of hydrogels.

For degradation evaluation, the hydrogels were incubated in type I collagenase (50 U/mL in PBS) at 37 °C. Initial weights ($m_{t\ =\ 0}$) of the hydrogels were determined after lyophilization. The samples were then incubated in a collagenase solution at 37 °C for 4 weeks. At predetermined time points (days 7, 14, 28), the samples were rinsed with ultrapure water, freeze dried and weighed again (m_t). The percent remaining weight was determined according to the following equation:

$$\text{Remaining} \cdot \text{weight} \cdot (\%) \cdot = \cdot \frac{m_t}{m_{t=0}} \times 100\% \quad (3)$$

These two tests were conducted in triplicate and the average values were calculated.

2.8. Measurement of rheological properties

The rheological property of hydrogels was investigated using a rheometer (MCR302, Anton Paar) with a temperature-controlled Peltier plate system. A 25 mm flat plate was used and the working gap distance was set at 1 mm. Silicone oil was placed around the plate to prevent water evaporation. Before measurements, disc-shaped specimens with 25 mm diameter and 1 mm thickness were printed and equilibrated in PBS. Firstly, oscillation strain sweep from 0.01 to 10% at a frequency of 1 Hz was performed to determine the linear viscoelastic region and 1% strain was chosen. Then, frequency sweep test was conducted from 0.1 to 10 Hz, and the storage modulus (G') and loss modulus (G'') were monitored. All tests were performed at 37 °C to simulate the physiological condition *in vivo*.

2.9. Cytocompatibility of hydrogels in vitro

L929 mouse fibroblast cells (L929), rabbit corneal epithelial cells (rCECs) and rabbit adipose-derived mesenchymal stem cells (rASCs) were used to test the cytocompatibility of hydrogels *in vitro*.

2.9.1. Cell culture

L929 cells were cultured in Dulbecco's Modified Eagle Media with 10% fetal bovine serum albumin and 1% penicillin/streptomycin. rCECs and rASCs were cultured in complete media provided by their corresponding company (BFB and Cyagen Company, China). All cells were cultured in a high humidity at 37 °C and 5% CO_2 on tissue culture polystyrene surface (TCPS). The cells were passaged and used for the cytocompatibility tests at 80% confluency by trypsin/EDTA solution.

2.9.2. MTT assay

The metabolic activity of cells co-cultured with hydrogels was investigated using the MTT assay. Approximately, the cells were seeded into 96-well plates with a density of 2×10^4 cells/well, incubated in 200 μL complete medium for 24 h, and then replaced with fresh media containing 50 μL sterilized hydrogels. After co-incubation for predetermined time, the media and hydrogels were discarded and refreshed with 180 μL complete media and 20 μL MTT solution (5 mg/mL). After 4 h, dimethyl sulfoxide (DMSO) was added into each well and the absorbance at 570 nm was recorded by a microplate reader (Infinite M200 PRO, Tecan, Switzerland). The cells without hydrogel were used as controls. Six parallel experiments were set up for each group of samples. The relative cell viability (%) was calculated with the reported protocol [37].

2.9.3. Live/dead (Calcein AM/PI) assay

To directly observe the viability of cells, the samples were stained using live/dead assay kit following manufacturer's protocol. The stained samples were observed using a fluorescence microscope (EVOS M5000, ThermoFisher Scientific) and images of live and dead cells stained with green and red respectively were captured.

2.9.4. 2D scratch assay

The scratch assay was performed according to previous reports [38, 39]. 5×10^4 cells were seeded on a 24-well plate and incubated until 80% confluency. Then, a scratch was made by a sterilized 200 μL pipette tip, and the sterilized hydrogel was added to the upper compartment. The cells without hydrogel treatment were used as controls. After 1 and 3 days, the cells were assessed by live/dead staining and the relative cell density within the scratched area was analyzed with Image J software.

2.9.5. Determination of cell adhesion

To assess the adhesion ability of the cells cultured on the hydrogels, the cells were seeded on the sterilized hydrogel in a 24-well plate and incubated for 2, 4, 6 days. At each time point, live/dead assay was conducted and CCK-8 was used to analyze cell proliferation on the surface of hydrogels. 50 μL CCK-8 and 450 μL complete media were added to each well and the cells were incubated in the dark for 4 h at 37 °C. After incubation, culture media were transferred to a new 96-well plate, and the absorbance at 450 nm was immediately read. Three samples were tested for each group.

2.9.6. 3D bioprinting and immunofluorescence staining

At an 80% confluency, the cells were passaged and uniformly suspended in the prepared ink solution under sterilized condition to yield a final concentration of 1×10^6 cells/mL. Then, the cell-laden precursor solution was transferred into ink box of DLP apparatus. Bioprinting conditions were set as layer thickness of 50 μm and curing time of 40 s. At 7 days after printing, the cell viability in hydrogel was determined via live/dead staining and analyzed by Image J software with the average number fraction of live cells reported. In addition, immunofluorescence staining was performed to verify the metabolic activity of cells in hydrogel. For rCECs, at 7 days after incubation, the 3D cell-laden constructs were fixed with a solution of 4% paraformaldehyde at room temperature for 2 h, rinsed with PBS and subsequently permeabilized in 0.5% Triton X-100 for 20 min and incubated with 2% bovine serum albumin for 15 min to block non-specific binding. The constructs were then incubated overnight at 4 °C with the primary antibody against cytokeratin 3 (CK3) (1:200, Bioss) and collagen type I (1:200, Bioss), and then incubated for 1 h in FITC-labelled secondary antibody (1:150, Bioss). Finally, the samples were co-stained with DAPI (Solarbio) and observed by a laser scanning confocal microscope (FV1200, Olympus). For rASCs, after 7 days incubation, the constructs were stained with collagen type I and phalloidin (Solarbio) as described above.

2.10. Nutrient diffusion tests

The nutrient permeability of hydrogel was carried out at 37 °C using a self-designed two-chamber device (Fig. S11). This device was composed of two symmetrical 8 mL diffusion chambers (donor and receptor) with an inner diameter of 18 mm. The donor and receptor chamber were filled with test solution and PBS, respectively. The equilibrated PEGDA-GelMA-20-5 hydrogel (thickness = 1 mm) was placed between the two chambers and fixed by the clamps on both sides. Firstly, the donor chamber was filled with methylene blue solution (1 mg/mL in PBS), a biological stain, to preliminarily investigate the diffusion ability of hydrogel. Photographs after 0, 0.5, 1, 1.5, 2, 24 h incubation were taken. Then, glucose (10 mg/mL in PBS) and bovine serum albumin (BSA, 10 mg/mL in PBS) solutions were respectively used to determine the nutrient permeability of the hydrogel. After glucose and BSA had diffused through the hydrogel for different time points, the solution in receptor chamber was homogeneously mixed by a syringe and a very small amount of solution was extracted to be used as samples. The glucose and BSA concentrations of samples were detected by a glucose content detection kit (Boxbio Biotechnology Co., Ltd) and a BCA protein assay kit (Boster Biotechnology Co., Ltd), respectively. The glucose and BSA solutions with different concentrations were used as the standard sample to prepare the calibration curves for quantification. The

test was conducted in triplicate and average values were calculated.

2.11. Printability of hydrogels

To verify the printability of PEGDA-GelMA hydrogels, different models including rabbit, crown, perforated disc, were printed and then photographed. The printing conditions were set as layer thickness of 50 μm and curing time of 20 s. To print cornea-shaped hydrogel, the concentration of photoabsorber and curing time were adjusted in the range of 0.05–0.15 wt%, and 10–80 s, respectively. Furthermore, to emulate the native structure of corneal stroma, the rCECs-laden hydrogel was printed into orthogonally aligned fibrous structure, photographed and evaluated by live/dead assay at 2 days post-printing. In order to evaluate the effect of photoabsorber on the printing fidelity, the ink in the presence of or absence of photoabsorber was prepared and the corresponding printed constructs were photographed.

2.12. In vivo assessment of hydrogel in a rabbit anterior lamellar keratoplasty (ALK) model

All the animal experiments were carried out according to the guidelines of the Tianjin Medical Experimental Animal Care, and animal protocols were approved by the Institutional Animal Care and Use Committee of Yi Shengyuan Gene Technology (Tianjin) Co., Ltd. (No. YSY-DWLL-2021010).

Hydrogel preparation: To imitate the natural structure of cornea, the PEGDA-GelMA-20-5 hydrogel was printed into two layers, including an epithelia layer (50 μm thick, 20 mm diameter) and an orthogonally aligned fibrous stroma layer (150 μm thick, 15 mm length of side). Printing conditions were set as layer thickness of 25 μm and curing time of 20 s. For cell-laden group, rCECs and rASCs were respectively encapsulated in the epithelia layer and stroma layer with the concentration of 1×10^6 cells/mL. Subsequently, the cell-laden and cell-free constructs were incubated in complete media at 37 °C and 5% CO_2 atmosphere, and PBS at room temperature, respectively. Media were refreshed every other day. At 4 days after printing, the bi-layer corneal scaffolds were used for the animal study. All the experimental procedures were performed under sterilized environment.

Surgical procedure: Twenty-one adult male rabbits (weighing about 2.5 kg) were randomly divided into three groups (seven rabbits per group), including cell-laden, cell-free hydrogel and control group (blank). All surgeries were performed on the right eyes of rabbits, and the left eyes were served as the normal group. The rabbits were firstly anesthetized through intramuscular injection of xylazine hydrochloride (0.2–0.3 mL) into thighs. Anterior lamellar keratoplasty was performed using a 3.5-mm customized vacuum trephine to cut a certain part of corneal epithelium-stroma and the collagen fibril layers were removed by a spatula. Then, the cell-laden or cell-free corneal scaffolds were punched with a trephine and carefully put on the corneal defect area with the printed epithelia layer facing upwards. Considering the risk of tearing the corneal scaffold by suturing, the construct was fixed with two 8-shaped overlying 10-0 sutures as previously reported method [40]. In the control group, only corneal defect was created and no hydrogel was placed. After surgery, a solution of floxacin was applied daily to prevent infection and to maintain moisture of the eye. The rabbits with free access to food and water were housed individually and kept under controlled temperature and humidity.

2.13. Slit-lamp biomicroscopy

Slit lamp (SLM-7E, Yimu Medical Technology Co., Ltd) was used to monitor the anterior ocular tissue at the predetermined time post-operation. With a × 16 magnification, using broad beam, the transparency of the hydrogel and surrounding cornea was evaluated. To assess the migration of the corneal epithelium over hydrogel and defect, cobalt blue slit lamp photography with fluorescein staining was performed.

2.14. Histological assessment

After explantation of the rabbit eyeballs, the samples were fixed in 4% (v/v) paraformaldehyde. Then, the sutures were gently removed and corneas were embedded in paraffin. The sections were stained with hematoxylin and eosin (H&E) for histological analysis. For immunofluorescence staining, paraffin sections (2–4 μm) were deparaffinized, rehydrated in ethanol and rinsed in PBS. Then 3% H_2O_2 was added and tissues were incubated at room temperature for 10 min. Nonspecific binding was blocked by incubation with goat serum for 10 min at 37 °C. The tissues were then incubated with primary antibody against cytokeratin 3 (CK3) (1:200, Bioss), collagen type I (Col I, 1:200, Bioss), lumican (LUM, 1:200, bioss) and alpha smooth muscle actin (SMA, 1:200, bioss) at 4 °C overnight. Detection was achieved by subsequent incubation with Alexa Fluor 488-conjugated secondary antibody (Solarbio) for 30 min at 37 °C. Then, the tissues were dehydrated, immersed in xylene, and scanned by a panoramic scanner (3DHISTECH P250 FLASH, 3DHISTECH).

2.15. Gene expression

To investigate the differentiation potential of implanted rASCs in the rabbit cornea, at 28 days post-surgery, 50 mg of wounded cornea was put into 1 mL Trizol (ThermoFisher Scientific) and homogenized thoroughly in a tissue grinder (KZ-III-F, Servicebio). Then, RNA from the samples was isolated by adding chloroform and centrifugation. The upper phase was collected and isopropanol was added, followed by centrifugation. The supernatant was discarded, and the RNA pellet was eluted into 75% ethanol, and then centrifugated. After removing the supernatant, the remaining pellet was air-dried, eluted, and quantitated using a Nanodrop 2000 (ThermoFisher Scientific). Enough RNA was obtained and transcribed to cDNA by using a quantitative reverse transcription kit (Takara) according to the manufacturer's protocol. The primers for the studied gene (Table S5) were added to sample cDNA and a real-time quantitative polymerase chain reaction (PCR) instrument (QuantStudio 1, ThermoFisher Scientific) was used with 40 amplification cycles. Normal cornea was defined as a reference for comparison. The relative fold change of gene expression was analyzed using the $2^{-\Delta\Delta Ct}$ method [10,16].

2.16. Statistical analysis

Data are expressed as the mean ± standard deviation. Statistical analysis was performed using two population student's t-test to evaluate the mechanical properties, cell migration, corneal thickness and PCR results. A value of $p < 0.05$ was considered statistically significant, and ns, *, **, ***, **** represent $p > 0.05$, $p < 0.05$, $p < 0.01$, $p < 0.001$, $p < 0.0001$, respectively. GraphPad Prism 8.0 Software was used to analyze the data.

3. Results and discussion

3.1. Preparation and characterizations of PEGDA-GelMA hydrogel

GelMA has been extensively studied for biomedical applications due to its conveniently photo-initiated gelling ability and biological activities to promote cellular attachment and growth [33]. Nevertheless, GelMA hydrogel is too brittle to be applied in corneal regeneration field. PEG is a kind of FDA-approved biocompatible polymers [41]. Herein, a long-chain PEGDA (Mn = 8 kg/mol) was copolymerized with GelMA to toughen the hydrogel system owing to the energy dissipating mechanism [42]. As shown in the ^1H nuclear magnetic resonance (NMR) spectra of PEGDA (Fig. S1) and GelMA (Fig. S2), new peaks appearing at 5.4–6.5 ppm were attributed to the grafted vinyl group. The

methacylation degree (MD) of GelMA was calculated as 75% through comparing the integrated areas of lysine methylene signals (3.0 ppm) in gelatin and GelMA spectra [35]. In the FTIR spectra of PEGDA and GelMA (Fig. S3), GelMA exhibited characteristic bands around 1229 cm^{-1} related to N-H deformation (amide III), 1542 cm^{-1} for N-H deformation (amide II), 1649 cm^{-1} for C=O stretching (amide I), 2933, 2863 cm^{-1} related to C-H stretching, and broad peak at 3285 cm^{-1} assigned to peptide bonds (mainly N-H stretching) and the stretching of the hydrogen bonded O-H [19,43]. The PEGDA showed the feature bands around 2879 cm^{-1} and 1734 cm^{-1} associated with C-H and C=O stretching, respectively. All these results confirmed the desired chemical structure of PEGDA and GelMA.

In this study, through DLP printing, we fixed the concentration of GelMA (5 wt%) and varied the PEGDA concentrations (i.e., 10, 15, and 20 wt%) to form hydrogels, and the resultant hydrogels were named as PEGDA-GelMA-10-5, PEGDA-GelMA-15-5, PEGDA-GelMA-20-5, respectively. The ^{1}H NMR spectra indicated that all characteristic peaks of vinyl group disappeared in hydrogels, proving the high efficiency of photoinitiated polymerization (Fig. S4). Next, the mechanical and other physical properties of hydrogels were assessed *in vitro* to determine the optimal concentration for producing a corneal scaffold with properties resembling most closely the native corneal tissue. All the samples were printed by DLP printer in the following measurement.

Firstly, the tensile and compressive tests were performed and results were exhibited in Fig. 2 and Table S1. As the concentration of PEGDA increased, the tensile strength and tensile modulus both showed an upward trend. In particular, the corresponding values of PEGDA-GelMA-20-5 hydrogel can respectively reach 82.2 kPa and 77.2 kPa, which were close to those of hydrogels applied in corneal regeneration, and favorable for cell encapsulation [44,45]. Besides, for the compressive test, although the addition of PEGDA had little effect on the improvement of modulus in comparison with the GelMA and PEGDA-GelMA hydrogels, it increased the toughness of GelMA hydrogel. When compressed by the mechanical test machine to 70% strain, the PEGDA-GelMA-20-5 hydrogel could keep the shape without breaking, but the GelMA hydrogel was broken during the compression process. Besides, the printed GelMA hydrogel with rough surface could not be picked up by a tweezer, whereas the PEGDA-GelMA-20-5 hydrogel demonstrated a high printing fidelity and could be easily handled with the tweezer. Comparatively, the compressive modulus of PEGDA-GelMA-20-5 (100.7 kPa) was close to that of the native cornea (115.3 kPa, Table S1) [44], which was crucial for resisting intraocular pressure in the native corneal environment and long-term tissue/biomaterial integration and remodeling.

To investigate the mechanism of mechanical improvement, X-ray diffraction (XRD) was performed. As shown in Fig. S5, the PEGDA and PEGDA-GelMA-20-5 hydrogel showed the characteristic peaks at 19° and 23°, which were in accordance with the previous report [46], whereas no peak appeared in the XRD pattern of GelMA at the corresponding angle. Thus, we considered that the physical crosslinks from crystalline domain of PEGDA resulted in the enhancement of toughness and strength [42]. Herein, we also examined the effect of the molecular weight of PEGDA on the mechanical strengths. We printed hydrogels with the PEGDA molecular weights of 3, 8, 10 and 20 kg/mol. It is noted that the 3D printed PEGDA(3k)-GelMA-20-5 hydrogel was easily broken when it was removed from the build platform, so the mechanical

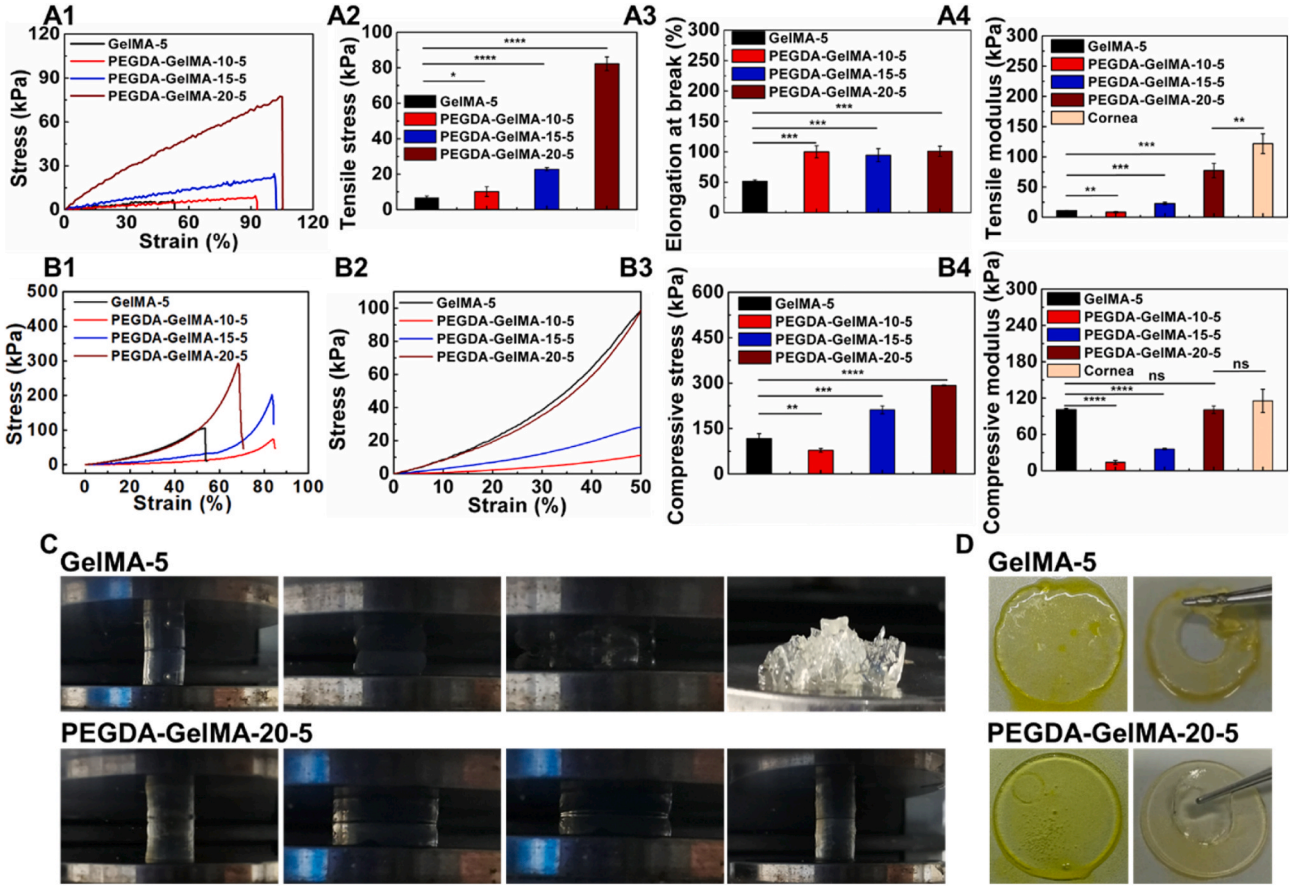

Fig. 2. Mechanical properties of GelMA and PEGDA-GelMA hydrogels. (A1) Representative tensile stress-strain curves and their corresponding (A2) tensile stress, (A3) elongation at break, and (A4) tensile modulus. (B1) Representative compressive stress-strain curves and their corresponding (B2) stress-strain curves before 50% strain, (B3) compressive stress, and (B4) compressive modulus. (C) Compressive process of GelMA-5 and PEGDA-GelMA-20-5 hydrogel by using a mechanical test machine. (D) Printed GelMA-5 and PEGDA-GelMA-20-5 hydrogel discs.

property of this hydrogel could not be measured on the testing machine. The reason is that the crosslinks from shorter PEGDA chains led to a fragile network. While the PEGDA(8k)-GelMA-20-5 achieved the highest tensile strength, modulus and an appropriate breaking strain. Nevertheless, further increasing molecular weight of PEGDA, the mechanical strengths dropped dramatically though the hydrogels maintained larger elongations at break (Fig. S6). The crosslinking with excessively longer PEGDA chains resulted in looser network; in this case, the formed hydrogel was too soft to support its own weight. Hence, 8 kg/mol molecular weight of PEGDA was selected to prepare PEGDA-GelMA hydrogel in the following test on account of its better comprehensive mechanical properties in terms of robustness and toughness.

The swelling behavior of hydrogels can indicate the degree of hydrophilicity and is an essential feature of the cornea. Phosphate buffered saline (PBS) was used here to simulate the *in vivo* physiological condition. Swelling experiment demonstrated that three proportions of hydrogels could reach equilibrium within 1 day, and obvious change of mass was not observed in the following two weeks. Besides, as the concentration of PEGDA increased, the swelling degree decreased, which was due to the formation of denser network and lower water permeability (Fig. 3A). In addition, in terms of application in keratoplasty, an implant with a stable swelling behavior can reduce the postoperative corneal deformation and pressure exerted by implant on the eyeball [45]. The water content of the cornea is closely related to its transparency and penetration capacity. Table S2 showed that the equilibrium water contents (EWCs) of hydrogels were in the range of 96–99%, well meeting the requirement of natural cornea (85%) [47].

A biomaterial used in the treatment of corneal defects is exposed to hydrolysis from matrix degrading enzymes produced by corneal keratocytes that participate in collagen fibril remodeling [48]. Hence, a tissue engineering scaffold needs to be biodegraded in a controlled manner. Next, type I collagenase (50 U/mL) was chosen to investigate the *in vitro* degradation profile of PEGDA-GelMA hydrogels. As depicted in Fig. 3B, all the hydrogels underwent different degrees of mass reduction. Only 41% PEGDA-GelMA-20-5 hydrogel was remained at 28 days. However, since the hydrogels became too soft and it was difficult to be separated with surrounding medium after immersing in collagenase solution, the degradation data of PEGDA-GelMA-10-5 hydrogel was only measured for 7 days. Nonetheless, the results suggested that the PEGDA-GelMA hydrogel could be degraded in collagenase solution, and a higher concentration of PEGDA led to a slower degradation rate since denser network inhibited penetration of collagenase. Thus, the

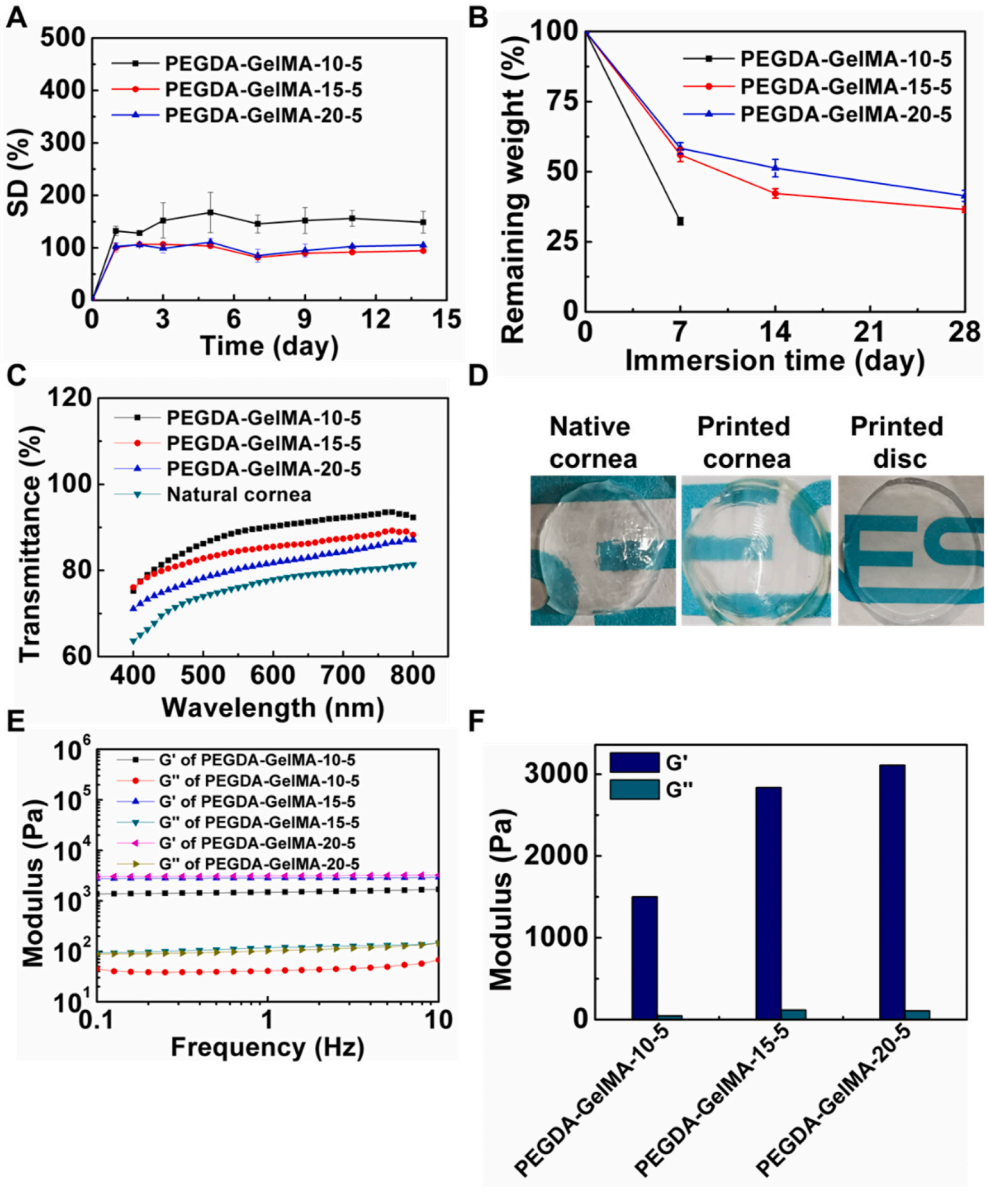

Fig. 3. Characterizations of PEGDA-GelMA hydrogels. (A) The swelling degree of the hydrogels after 14 days incubation in PBS at 37 °C. (B) Degradation curve of the hydrogels in the presence of collagenase (50 U/mL) in PBS at 37 °C. (C) Optical transmittance of hydrogels and natural cornea between 400 and 800 nm. (D) Photographs showing transparency of native cornea, printed cornea and printed disc. (E) Frequency sweep curves of hydrogels at a frequency range from 0.1 to 10 Hz. (F) Averaged storage modulus (G') and loss modulus (G'') calculated from (E).

PEGDA-GelMA hydrogel could be applied as a tissue engineering scaffold, which would be gradually degraded to induce tissue integration and achieve the new corneal tissue regeneration.

Transparency is an important factor that should be taken into account for designing a corneal tissue scaffold. The light transmittance of the PEGDA-GelMA hydrogel and native cornea was determined at the visible light wavelength ranging from 400 to 800 nm. The PEGDA-GelMA hydrogel exhibited a higher transparency than native cornea in the visible region (Fig. 3C), and PEGDA-GelMA-10-5, PEGDA-GelMA-15-5, PEGDA-GelMA-20-5 hydrogel possessed 90.7%, 86.3%, 82.5% light transmittance at 600 nm, respectively, larger than that of native cornea (77.9%, Table S2). The reduced transparency of hydrogel with the increment of PEGDA concentration was possibly due to the light scattering resulted from emulsification when excessive PEGDA was mixed with GelMA. Fig. 3D displayed the photographs of native cornea, printed corneal scaffold, and printed disc. Letters below the printed constructs were clearly visible, proving the superior transparency of the PEGDA-GelMA hydrogel.

Rheological tests were then performed to examine the viscoelastic properties of PEGDA-GelMA hydrogels (Fig. 3E and F and Table S2). Firstly, the hydrogels were subjected to strain sweep to determine the linear viscoelastic region (Fig. S7), and 1% strain was chosen for the following frequency sweep examination from 0.1 to 10 Hz. The PEGDA-GelMA-10-5, PEGDA-GelMA-15-5, PEGDA-GelMA-20-5 hydrogel showed averaged storage modulus (G') of 1.5, 2.8, 3.1 kPa, respectively, among which the value of PEGDA-GelMA-20-5 hydrogel was close to that of native cornea (~4 kPa) [15]. Throughout the screened frequency range, the G' was consistently higher than the loss modulus (G''), suggesting that all hydrogels were stable and maintained gel state. The tanδ, which represented the ratio of loss modulus to storage modulus, was found to be significantly less than 1 (0.02–0.05), suggesting the elastic character of PEGDA-GelMA hydrogel required for designing a corneal scaffold (tanδ = 0.25) [15].

3.2. *Cytocompatibility and nutrient permeability of PEGDA-GelMA hydrogel*

To evaluate the cytocompatibility of PEGDA-GelMA hydrogels, L929 mouse fibroblast cells (L929), the prevalent cell line employed in cytotoxicity assay, were preliminarily used. As shown in Fig. S8, after co-

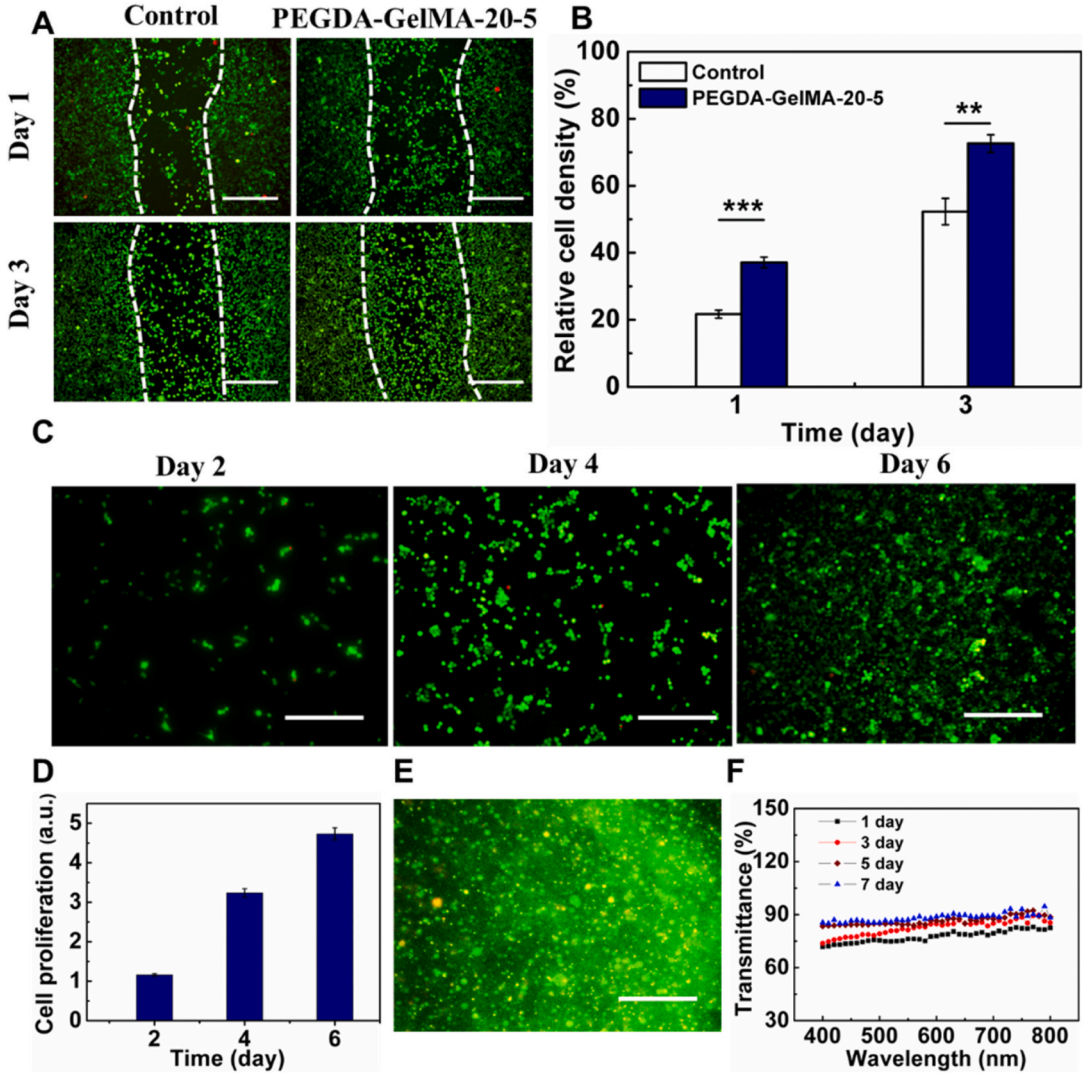

Fig. 4. *In vitro* cytocompatibility of PEGDA-GelMA-20-5 hydrogel. (A) Representative live/dead images of rCECs in 2D scratch assay. (B) Quantification of relative cell density in the scratched area in the hydrogel and control samples. (C) Representative live/dead images of rCECs seeded on the surface of PEGDA-GelMA-20-5 hydrogel. (D) CCK-8 results of the cell proliferation on the hydrogel. (E) Representative live/dead image of rCECs encapsulated in the hydrogel at 7 days after bioprinting. (F) Transparency change of the rCECs-loaded hydrogels between 400 and 800 nm at 1, 3, 5, 7 days after bioprinting. Scale bars in live/dead images: 300 μm.

incubation of hydrogels with L929 for 1, 3 days, the cell viabilities of all groups could reach 90% and cells maintained normal morphology and proliferation capability. After 2 days culture, the PEGDA-GelMA-20-5 hydrogel supported L929 adhesion, and almost all the cells were flattened with a spread morphology and protrusion, which was typical morphology of attached cells. Live/dead images further demonstrated the high viability of L929 cells on the surface of hydrogel.

To explore its application in corneal regeneration, we next mainly focused on the evaluation of cytocompatibility with rabbit corneal epithelial cells (rCECs), including cytotoxicity, cell migration, adhesion, proliferation, and cell viability after bioprinting. Firstly, the cytotoxicity test was performed using MTT and live/dead assay. Fig. S9 showed that above 90% cell viability was observed over 5 days incubation. The rCECs maintained normal proliferation capability in the presence of hydrogels. As discussed above, the PEGDA-GelMA-20-5 hydrogel possessed sufficient mechanical strength, printing shape fidelity, high light transmittance, suitable swelling degree and degradation rate, which all met the requirement of the corneal scaffold. Hence, the PEGDA-GelMA-20-5 hydrogel was chosen for the following measurements.

Cell migration ability is important in wound healing process. The *in vitro* scratch assay revealed that the rCECs on the surface of tissue culture polystyrene surface (TCPS) and PEGDA-GelMA-20-5 hydrogel could migrate to the scratched area (300–600 μm distance) over 3 days (Fig. 4A). To quantify the migration degree to the wounded area, the relative cell density in the scratched area was calculated, and the corresponding values for TCPS and PEGDA-GelMA-20-5 group were respectively 52% and 73% after 3 days incubation, demonstrating that the cells on the surface of hydrogel showed a higher migration ability than those on the TCPS (Fig. 4B). This was attributable to the porous structure of hydrogel, which not only promoted the transportation of nutrients and metabolites, but also provided large space for cell proliferation and migration.

The ability of a scaffold to support cell adhesion is also vital for tissue regeneration. In the following experiment, the rCECs were seeded on the surface of PEGDA-GelMA-20-5 hydrogel, followed by the live/dead and CCK-8 assay. As shown in Fig. 4C and D, the cells exhibited a higher adhesion and proliferation ability, which was resulted from the bioactivity of GelMA. After 6 days, the cell number on the hydrogel surface was 4.7-fold as that at 2 days.

To examine the influence of printing on cell viability, the rCECs were encapsulated in the gel precursor solution at 1×10^6 cells/mL concentration to form a bioink, which was printed and then incubated in the rCECs culture medium for 7 days. The cell viability was estimated using the live/dead assay (Fig. 4E). There was negligible cell death during the printing process, and the viability of rCECs in the printed construct was found to be 90% using the Image J software. The cells were distributed uniformly and not aggregated in the printed hydrogel. Thus, the bioink and printing did not affect the viability of the encapsulated cells. After culturing for 7 days, the expressions of type I collagen (Col I, the main component of corneal extracellular matrix (ECM)) [49] and cytokeratin 3 (CK3, corneal epithelial-specific protein) [50] within hydrogel were investigated by immunofluorescence (IF) staining and confocal microscopy. As shown in Fig. S10, the Col I and CK3 were noticeably expressed in the hydrogel, indicating that the rCECs retained their phenotype and metabolic activity.

According to the previous report, the existence of cells would cause light scattering, thus reducing the transmittance of hydrogels [35]. So, optical transmittance of cell-loaded hydrogel after 1, 3, 5, 7 days incubation was measured in the following tests (Fig. 4F). It is observed that the transmittance increased within 7 days (77.8%, 84,7%, 86.5%, 88.9% at 600 nm for 1, 3, 5, 7 days, respectively), which was possibly due to the exudation of photoabsorber during the incubation process. It is worth noting that although the cells were encapsulated and the hydrogels were immersed in the culture medium, the transparency of the constructs still met the requirement of corneal scaffold.

Nutrient transport throughout tissue engineering scaffold is critical for cell survival and proper function. Here, nutrient penetration ability of PEGDA-GelMA-20-5 hydrogel was investigated. Methylene blue solution was used to preliminarily examine the diffusion property. The results showed that after 24 h incubation at 37 °C, blue color in the receptor chamber became deeper, indicating the successful penetration of methylene blue through the hydrogel film (Fig. S11A). Thereafter, glucose and BSA were used as the representative nutrients to examine the nutrient diffusion ability of hydrogel. On the basis of Fick's law of diffusion, calibration curves (Figs. S11B and C) and permeation curves (Fig. S11D), the diffusion coefficients of PEGDA-GelMA-20-5 hydrogel for glucose and BSA were calculated as 2.97×10^{-6} cm^2/s and 1.46×10^{-6} cm^2/s (see SI), respectively, which were close to those of human cornea (3.00×10^{-6} cm^2/s, and 1.10×10^{-6} cm^2/s, respectively) [51, 52]. The results indicated that the PEGDA-GelMA-20-5 hydrogel possessed similar permeation property to native cornea, which was conductive to corneal regeneration.

3.3. Printability evaluation of PEGDA-GelMA hydrogel

In order to investigate the applicability of PEGDA-GelMA-20-5 precursor solution as 3D printing bioink, the DLP printer and different kinds of models were utilized. As depicted in Fig. 5, after layer-by-layer photocuring, rabbit (Fig. 5A2), perforated disc (Fig. 5B1), and crowns with hollow structure (Fig. 5C2) were successfully printed out. Although yellow color post-printing was observed due to the presence of photoabsorber, the objects became colorless and transparent after immersion in PBS (Fig. 5C3 and C4). Additionally, the holes in the perforated disc under a microscope were uniform (Fig. 5B2), and the printed crown was mechanically strong enough to keep the hollow structure from collapsing (Fig. 5C3 and C4), indicating its high fidelity. Next, to simulate the structure of native corneal stroma, orthogonally aligned fibrous model was established and printed constructs displayed orthogonal stripes whether in macro- or microscale (Fig. 5D2 and D3). At 2 days after bioprinting, the rCECs encapsulated in the hydrogels were evenly distributed and showed high viability (Fig. 5D4), and the cells-loaded hydrogels could be picked up by a tweezer without collapsing after immersing in the culture medium (Fig. 5E). To inspect the influence of photoabsorber on printing fidelity, the ink with or without photoabsorber was printed, and corresponding constructs were shown in Fig. 5F1 and F2. It is noticed that the hydrogels containing photoabsorber exhibited clear border and smooth surface, whereas coarse surface was displayed in the printed hydrogel in the absence of photoabsorber, indicating overexposure happened when the photoabsorber was not included in the ink system.

Cornea has dome-shaped structure, which is difficult to be printed. We next explored the feasibility of using rCECs-laden PEGDA-GelMA-20-5 precursor solution as bioink to print cornea-shaped structure. The programmed 3D geometry of rabbit's cornea was sliced to generate a stack of cross-section images, so the dome-shaped cornea led to the projection of a disc and a series of annulus slices. In our study, the layer thickness was fixed at 50 μm, and curing time and photoabsorber concentration were optimized to print constructs with the highest fidelity. Tables S3 and S4 and Fig. 5G showed the printing parameters and results of cell-free and rCECs-laden printed constructs. It can be summarized as follows: (1) curing time should be long enough to solidify bioink (Table S3, serial number 1 and 2, serial number 3 and 4); (2) photoabsorber concentration influenced the printing fidelity. When it was too low, overexposure happened (Table S4, serial number 1), and in contrast, when it was too high, solidification was incomplete (Table S4, serial number 2); (3) encapsulated rCECs exerted a contraction force on the construct (Table S4, serial number 3, 4, 5); (4) the most appropriate printing parameters were 40 s curing time, 0.15 wt% photoabsorber concentration, and 80 s curing time, 0.1 wt% photoabsorber concentration for cell-free and rCECs-laden corneal constructs, respectively.

The above results demonstrated that it was feasible to bioprint dome-shaped rCECs-loaded 3D corneal scaffold without additional supporting

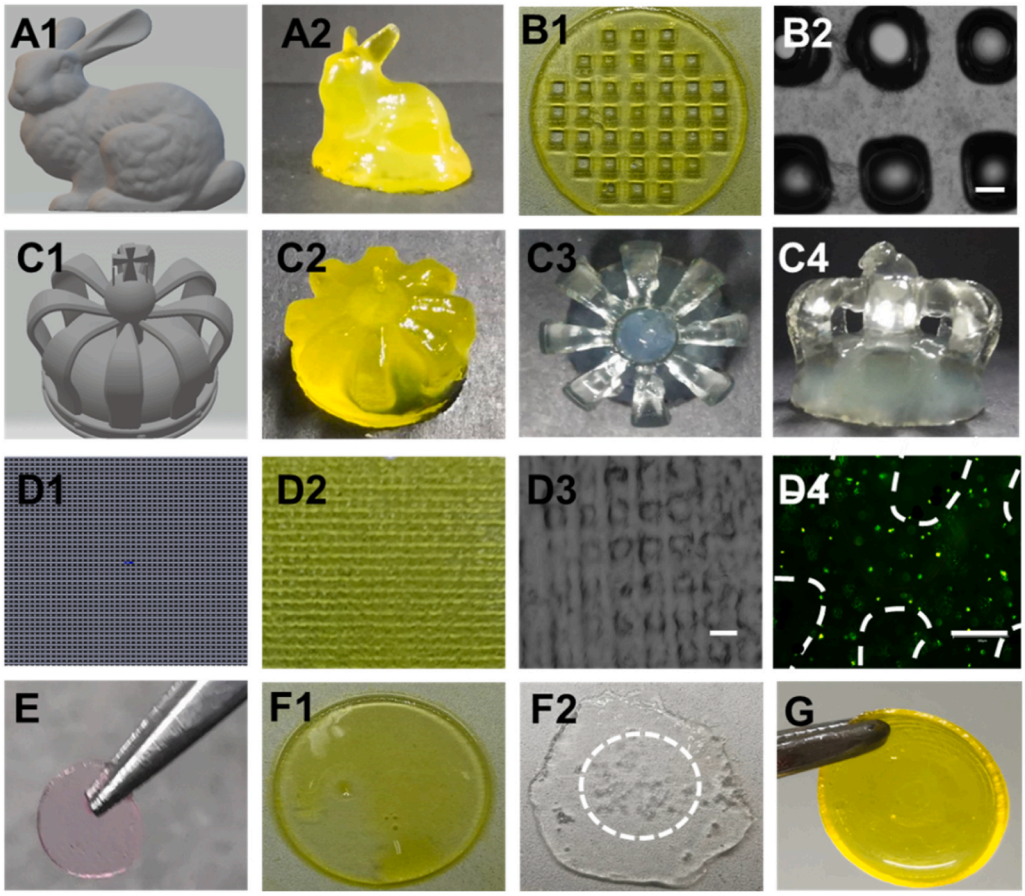

Fig. 5. Printability evaluation of PEGDA-GelMA-20-5 hydrogel. (A1) 3D model and (A2) digital photo of printed rabbit. (B1) Digital photo and (B2) micrograph of printed perforated disc. (C1) 3D model and (C2) digital photo of printed crown. (C3) Top view and (C4) side view of crown after immersion in PBS. (D1) 3D model, (D2) digital photo and (D3) micrograph of printed orthogonally aligned fibrous structure. (D4) Evaluation of live/dead rCECs viability in orthogonally aligned fibrous object after culturing for 2 days. (E) Printed hydrogel after immersion in cell culture medium for 2 days. Printed hydrogel disc (F1) with and (F2) without photoabsorber. White circle denoted the predetermined printing area. (G) Printed corneal scaffold. Scale bars: 300 μm.

apparatus. The DLP printing provided a robust strategy that allowed for printing tissue scaffolds with complex geometries using cell-friendly bioinks and avoiding the need for additional curing steps post-printing. In clinic, the curvature and thickness can also be regulated and customized with 3D printing technology to fabricate a patient-specific artificial cornea, indicating the great application potential of this bioink system in corneal regeneration.

3.4. In vivo assessment of 3D printed bi-layer cornea scaffold in a rabbit anterior lamellar keratoplasty (ALK) model

When cornea is damaged, it is vital to accelerate the regeneration of both corneal epithelium and stroma. Based on the desired comprehensive properties discussed above, next, a bi-layer corneal scaffold was used in the New Zealand rabbit model of corneal lamellar transplant in the following animal experiment, and its biocompatibility and biointegration for repair and sealing of corneal defects were evaluated. In our study, the rCECs and rabbit adipose-derived mesenchymal stem cells (rASCs) were chosen as cell sources for repair of epithelium and stroma layer, respectively. The rCECs were used to treat potential limbal stem cells (LSC) deficiency disease, and rASCs were used taking into account its ability to mitigate inflammation and differentiate into corneal stromal cells in situ [53]. Firstly, the cytocompatibility of PEGDA-GelMA-20-5 hydrogel with rASCs was examined by performing MTT assay, live/dead staining and immunofluorescence staining. As depicted in Fig. S12, the rASCs showed high viability after co-culturing with hydrogel. After 7 days of culturing, elongation and spreading of encapsulated rASCs were observed, and the rASCs secreted Col I normally. In the animal study, to emulate the natural structure of cornea, a bi-layer construct consisting of rCECs-laden epithelium layer and a rASCs-laden orthogonally aligned fibrous stroma layer was printed. The orthogonally aligned fibrous structure was printed to recapitulate fibrous structure of the native corneal stroma, which would provide the hierarchical and morphological cues to facilitate the growth and differentiation of the loaded cells [10,54]. Fig. 6A exhibited that the cornea was wounded with a customized 3.5-mm vacuum trephine, and then 3D printed cell-laden or cell-free PEGDA-GelMA-20-5 hydrogel was put on the wounded area. Finally, two 8-shaped overlying sutures were used to hold the scaffold in place as reported previously [40]. During the whole implantation process, the scaffold was robust enough to be handled without collapse. As a control, only corneal defect was created and no hydrogel was implanted onto the recipient bed.

Slit lamp examination was then conducted at the predetermined time points after surgery and results were exhibited in Fig. 6B. The implanted hydrogel remained transparent during the whole 28 days in the cell-laden and cell-free groups, and no obvious inflammation and neovascularization was observed. The cornea preserved a smooth surface and complete curve, demonstrating that all implants remained in place during the whole observation period, and there was no visible scar on the cornea. Additionally, cobalt blue slit lamp photographing with fluorescein staining was performed to investigate whether there was migration of the epithelium over the hydrogel or wounded area. The results showed that corneal epithelial defect (green area) underwent progressive reduction, suggesting the successful epithelization. In the cell-laden and cell-free group, the corneal epithelial defect was completely healed within 7 days, whereas 14–21 days were needed for control group to epithelization, indicating an efficient therapeutic effect of hydrogel in promoting corneal wound healing. During the observation period, the graft was firmly held without dislocation, demonstrating the efficacy of overlying suture method and biointegration of implanted scaffold with native tissue.

Histological H&E staining and immunofluorescence staining are

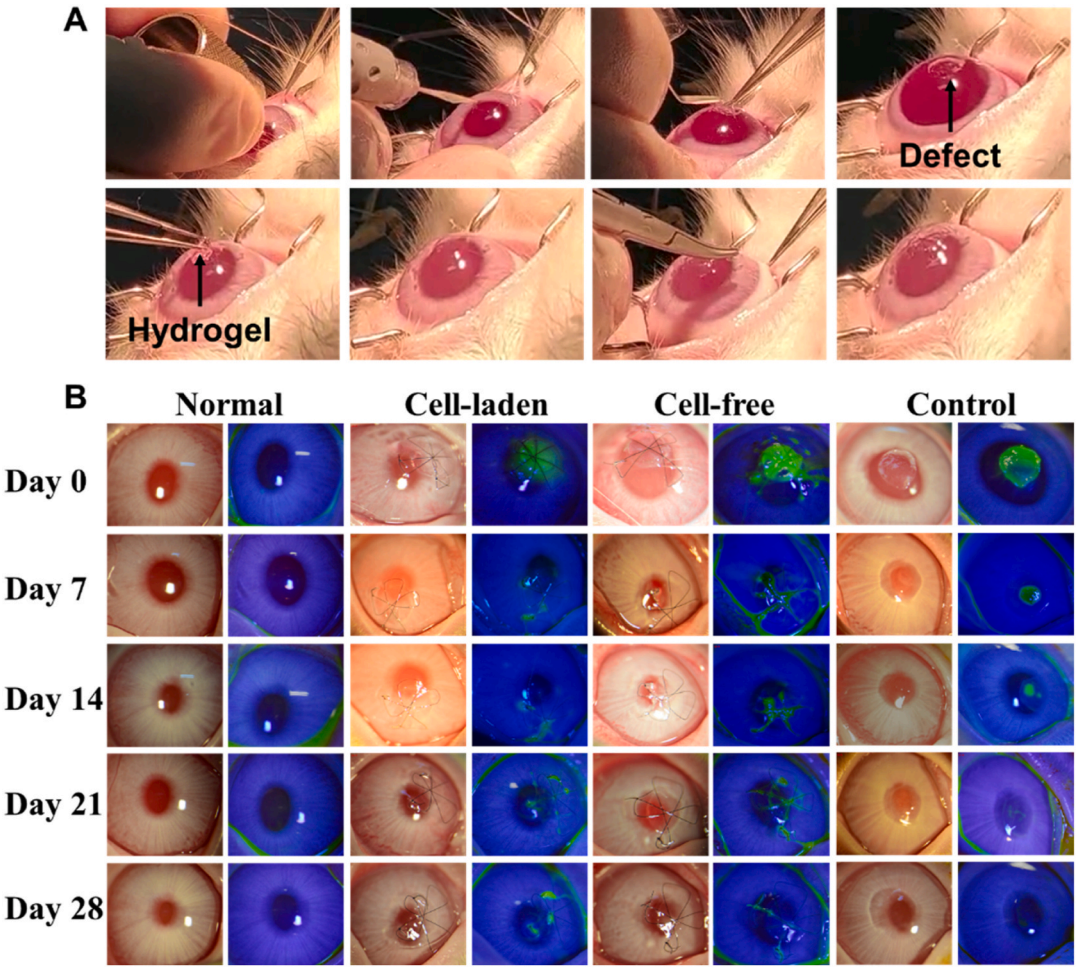

Fig. 6. *In vivo* evaluation of the 3D printed bi-layer corneal scaffold in a rabbit model of ALK. (A) Surgical procedures of keratoplasty, including removing a certain part of corneal epithelium-stroma by a trephine and spatula, implantation of the hydrogel, and overlying suture. (B) Representative slit lamp and cobalt blue photographs after *in vivo* application of hydrogel to rabbit cornea at different time points. Progressive reduction in the size of corneal epithelial defect (green area in the central cornea) implicated epithelial migration over hydrogel and defect.

shown in Fig. 7. At 1 day post-surgery (Fig. 7A), stroma hyperplasia was observed in H&E staining of cell-laden, cell-free and control groups, which probably resulted from inflammation or infection after keratoplasty. Similar to normal group, the remaining stroma still exhibited fibrous collagen type I structure. The epithelium layer of cornea was verified to be dissected according to the CK3 staining results. It is worth noting that the hydrogel was not observed in the histological results possibly due to its detachment from the wounds during manipulation of the corneas for fixation and histological analysis. It is evident that at this time the hydrogel was not completely integrated with the recipient bed at 1 day. After 28 days, the thicknesses of total, epithelium and stroma layer of cornea in cell-laden, cell-free and control groups (Fig. 7B1 and C) were comparable to those of native cornea except for the epithelium thickness in control group, indicating that stroma hyperplasia had been alleviated and the epithelial layer in untreated samples could not be regenerated completely. Additionally, the implanted scaffold was not discernible owing to biodegradation. In this case, the scaffold was entirely replaced by dense stromal tissue, suggesting that the bi-layer corneal scaffold was seamlessly integrated with the recipient corneal bed. Col I and CK3 immunostaining (Fig. 7B2 and B3) both revealed that the cell-laden and cell-free scaffold could induce the regeneration of the epithelium and stroma better than the control group. The aligned fibrous collagen and CK3 were produced in the cell-laden and cell-free group. The stroma in the operated area appeared normal. The inflammatory cell infiltration or apparent scarring was not observed in histological images. The corneal epithelium over the graft was well stratified, which was similar to that in the normal cornea. However, incomplete epithelization and stroma regeneration were detected in control group (denoted by red arrows and rectangles), and disordered collagen fibrous structure was present in the regenerated stroma region, demonstrating the printed orthogonally aligned fibrous structure can help induce the specific growth of ECM [55,56]. Based on the previous report [3], damaged cornea led to the activation of quiescent keratocytes that transformed into fibroblasts and myofibroblasts, eliciting secretion of large amount of randomly organized collagen fibers to repair the wound. As a result, the randomly organized fibers caused light scattering and thus deterioration of vision. Hence, lumican (LUM, aiding in ECM organization, abundantly expressed by corneal keratocyte) and α-smooth muscle actin (SMA, producing abnormal ECM and inducing tissue contraction, scar formation and corneal opacity) immunofluorescence stainings (Fig. 7B4 and B5) were conducted to investigate the keratocyte phenotype in wounded area [16,57]. It is demonstrated that LUM was abundantly expressed in corneas implanted with bilayer scaffold, which was similar to the normal cornea, whereas lower fluorescence intensity was observed in control group (denoted by red rectangle). In comparison, more expression of LUM was detected in cell-laden group compared with cell-free group, indicating that the encapsulated rASCs differentiated into keratocyte in the corneal microenvironment. Moreover, more SMA was expressed in the wounded area without hydrogel treatment, suggesting that the keratocytes close to the wounded area were activated

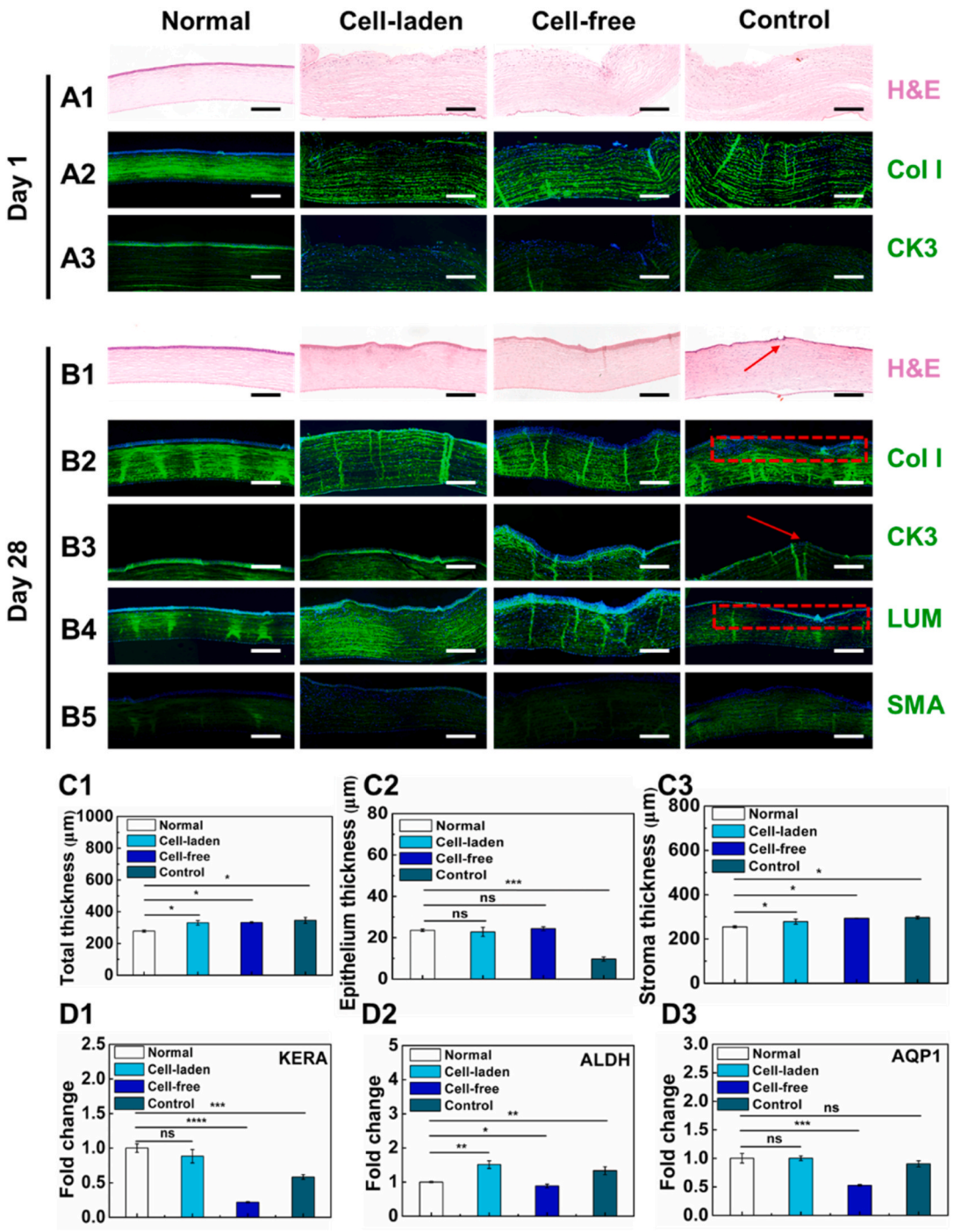

Fig. 7. Histological and gene expression analysis after application of the 3D printed bi-layer corneal scaffold in a rabbit model of ALK. (A1) H&E staining and immunostaining with (A2) Col I and (A3) CK3 antibodies (green) of the corneas at 1 day post-surgery. (B1) H&E staining and immunostaining with (B2) Col I, (B3) CK3, (B4) LUM, and (B5) SMA antibodies (green) at 28 days post-surgery. The red arrows and rectangles denoted the uncompleted epithelium and stroma region, respectively. In all images, nuclei were co-stained with DAPI (blue). The scale bars were 200 μm. Thickness of (C1) total, (C2) epithelium, and (C3) stroma layer of cornea at 28 days post-surgery obtained from H&E images. The relative gene expressions of (D1) KERA, (D2) ALDH, (D3) AQP1 in corneas, which were quantified by PCR at 28 days post-surgery. Values reflected fold change in mRNA expression over normal cornea.

and differentiated into SMA-positive myofibroblasts. However, the bi-layer corneal scaffold significantly restrained the expression of SMA, which was conductive to avoiding myofibroblast formation and corneal scarring.

To further verify the differentiation potential of the encapsulated rASCs in the hydrogel after keratoplasty, the gene expressions of the keratocytes specific markers keratocan (KERA), ALDH3A1 (ALDH) and aquaporin (AQP1) were assessed by polymerase chain reaction (PCR) technology (the corresponding primer sequences were shown in Table S5) [10]. From the results shown in Fig. 7D, the expressions of the three genes in cell-laden group were comparable to those in normal group. There was no statistical difference in the expressions of KERA and AQP1 between the two groups. However, lower expression was observed in cell-free and control group, which indicated that keratocyte-related gene expression was restricted, further proving that the encapsulated rASCs differentiated into keratocyte in the corneal microenvironment

and these stem cells could facilitate the corneal regeneration. Taken together, the synergistic effects of orthogonally aligned fibrous structure and encapsulated stem cells could provide an appropriate topographical and biological microenvironment for guiding the correct corneal regeneration pathway.

4. Conclusions

We developed a two-component ink composed of GelMA and long-chain PEGDA. Copolymerization of long-chain PEGDA with GelMA could contribute to formation of a robust PEGDA-GelMA hydrogel, resolving the intrinsic brittleness of GelMA hydrogel, owing to the toughening effect from the crystalline crosslinking of PEGDA chain. Diverse objects of PEGDA-GelMA hydrogels could be customized by DLP printing technology. The 3D printed PEGDA-GelMA hydrogels were shown to be cytocompatible and meet the requirements of corneal implant in terms of supporting cell adhesion, proliferation, and migration, as well as a high light transmittance, an appropriate swelling degree, nutrient permeation and degradation rate. We printed a bi-layer dome-shaped corneal implant consisting of epithelia layer bearing rabbit corneal epithelial cells (rCECs) and orthogonally aligned fibrous stroma layer loading rabbit adipose-derived mesenchymal stem cells (rASCs), recapitulating microstructure and microenvironment of natural cornea. This bi-layer cells-laden corneal construct was applied in a rabbit anterior lamellar keratoplasty (ALK) model. We demonstrated that the 3D printed biomimetic epithelium/stroma bilayer hydrogel implant could facilitate the corneal regeneration with efficient re-epithelialization and stromal regeneration. In the future, suture resistance of this hydrogel needs to be further improved. Clinically, biomimetic endothelium layer construction should also be taken into account to realize the whole corneal regeneration.

CRediT authorship contribution statement

Binbin He: Investigation, Data curation, Methodology, Formal analysis, Writing – original draft. **Jie Wang:** Investigation, Data curation, Methodology. **Mengtian Xie:** Software, Investigation, Data curation. **Miaoyi Xu:** Software, Investigation, Data curation. **Yahan Zhang:** Investigation, Data curation. **Huijie Hao:** Resources, Data curation. **Xiaoli Xing:** Resources, Data curation. **William Lu:** Resources, Data curation. **Quanhong Han:** Investigation, Data curation, Methodology. **Wenguang Liu:** Conceptualization, Formal analysis, Writing – review & editing.

Declaration of competing interest

The authors declare that they have no known competing financial interests or personal relationships that could have appeared to influence the work reported in this paper.

Acknowledgments

The authors gratefully acknowledge the support for this work from National Key Research and Development Program (Grant No. 2018YFA0703100) and National Nature Science Foundation of China (Grant No. 51733006).

Appendix A. Supplementary data

Supplementary data to this article can be found online at https://doi.org/10.1016/j.bioactmat.2022.01.034.

References

[1] A.O. Eghrari, S.A. Riazuddin, J.D. Gottsch, Overview of the cornea: structure, function, and development, Prog. Mol. Biol. Transl. 134 (2015) 7–23.
[2] B. Kong, W. Sun, G. Chen, S. Tang, M. Li, Z. Shao, S. Mi, Tissue-engineered cornea constructed with compressed collagen and laser-perforated electrospun mat, Sci. Rep. 7 (1) (2017) 970.
[3] S. Chaurasia, R. Lim, R. Lakshminarayanan, R. Mohan, Nanomedicine approaches for corneal diseases, J. Funct. Biomater. 6 (2) (2015) 277–298.
[4] P. Gain, R. Jullienne, Z. He, M. Aldossary, S. Acquart, F. Cognasse, G. Thuret, Global survey of corneal transplantation and eye banking, JAMA Ophthalmol. 134 (2) (2016) 167–173.
[5] W.B. Lee, R.M. Shtein, S.C. Kaufman, S.X. Deng, M.I. Rosenblatt, Boston keratoprosthesis: outcomes and complications, Ophthalmology 122 (7) (2015) 1504–1511.
[6] M. Nouri, H. Terada, E.C. Alfonso, C.S. Foster, M.L. Durand, C.H. Dohlman, Endophthalmitis after keratoprosthesis: incidence, bacterial causes, and risk factors, Arch. Ophthalmol. 119 (4) (2001) 484–489.
[7] R. Viitala, V. Franklin, D. Green, C. Liu, A. Lloyd, B. Tighe, Towards a synthetic osteo-odonto-keratoprosthesis, Acta Biomater. 5 (1) (2009) 438–452.
[8] A. Isidan, S. Liu, P. Li, M. Lashmet, L.J. Smith, H. Hara, D.K.C. Cooper, B. Ekser, Decellularization methods for developing porcine corneal xenografts and future perspectives, Xenotransplantation 26 (6) (2019), e12564.
[9] I. Anton-Sales, J.C. D'Antin, J. Fernández-Engroba, V. Charoenrook, A. Laromaine, A. Roig, R. Michael, Bacterial nanocellulose as a corneal bandage material: a comparison with amniotic membrane, Biomater. Sci. 8 (10) (2020) 2921–2930.
[10] B. Kong, Y. Chen, R. Liu, X. Liu, C. Liu, Z. Shao, L. Xiong, X. Liu, W. Sun, S. Mi, Fiber reinforced GelMA hydrogel to induce the regeneration of corneal stroma, Nat. Commun. 11 (1) (2020), 1435–1435.
[11] B.C. Kilic, V. Hasirci, Cell loaded 3D bioprinted GelMA hydrogels for corneal stroma engineering, Biomater. Sci. 8 (1) (2019) 438–449.
[12] A. Gautieri, S. Vesentini, A. Redaelli, M.J. Buehler, Hierarchical structure and nanomechanics of collagen microfibrils from the atomistic scale up, Nano Lett. 11 (2) (2011) 757–766.
[13] Z. Chen, X. Liu, J. You, Y. Song, E. Tomaskovic-Crook, G. Sutton, J.M. Crook, G. G. Wallace, Biomimetic corneal stroma using electro-compacted collagen, Acta Biomater. 113 (1) (2020) 360–371.
[14] S. Majumdar, X. Wang, S.D. Sommerfeld, J.J. Chae, E. Athanasopoulou, L. S. Shores, X. Duan, L.M. Amzel, F. Stellacci, O. Schein, Q. Guo, A. Singh, J. H. Elisseeff, Cyclodextrin modulated type I collagen self-assembly to engineer biomimetic cornea implants, Adv. Funct. Mater. 28 (41) (2018), 1804076.
[15] F. Chen, P. Le, G.M. Fernandes-Cunha, S.C. Heilshorn, D. Myung, Bio-orthogonally crosslinked hyaluronate-collagen hydrogel for suture-free corneal defect repair, Biomaterials 255 (2020), 120176.
[16] L. Koivusalo, M. Kauppila, S. Samanta, V.S. Parihar, T. Ilmarinen, S. Miettinen, O. P. Oommen, H. Skottman, Tissue adhesive hyaluronic acid hydrogels for sutureless stem cell delivery and regeneration of corneal epithelium and stroma, Biomaterials 225 (2019), 119516.
[17] B. Zhang, Q. Xue, H. Hu, M. Yu, L. Gao, Y. Luo, Y. Li, J. Li, L. Ma, Y. Yao, H. Yang, Integrated 3D bioprinting-based geometry-control strategy for fabricating corneal substitutes, J. Zhejiang Univ. - Sci. B 20 (12) (2019) 945–959.
[18] A. Bidaguren, J. Mendicute, I. Madarieta, N. Garagorri, Confocal and histological features after poly(ethylene glycol) diacrylate corneal inlay implantation, Transl. Vis. Sci. Technol. 8 (6) (2019) 39.
[19] C. Kilic Bektas, V. Hasirci, Cell loaded GelMA: HEMA IPN hydrogels for corneal stroma engineering, J. Mater. Sci. Mater. Med. 31 (1) (2020) 2.
[20] M. Fuest, G.H. Yam, J.S. Mehta, D.F. Duarte Campos, Prospects and challenges of translational corneal bioprinting, Bioengineering 7 (3) (2020) 71.
[21] M. Ahearne, J. Fernández Pérez, S. Masterton, P.W. Madden, P. Bhattacharjee, Designing scaffolds for corneal regeneration, Adv. Funct. Mater. 30 (44) (2020), 1908996.
[22] I. Tsai, C. Hsu, K. Hung, C. Chang, Y. Cheng, Applications of biomaterials in corneal wound healing, J. Chin. Med. Assoc. 78 (4) (2015) 212–217.
[23] F. Rengier, A. Mehndiratta, H. von Tengg-Kobligk, C.M. Zechmann, R. Unterhinninghofen, H.U. Kauczor, F.L. Giesel, 3D printing based on imaging data: review of medical applications, Int. J. Comput. Assist. Radiat. 5 (4) (2010) 335–341.
[24] C. Schubert, M.C. van Langeveld, L.A. Donoso, Innovations in 3D printing: a 3D overview from optics to organs, Br. J. Ophthalmol. 98 (2) (2014) 159–161.
[25] D. Chimene, R. Kaunas, A.K. Gaharwar, Hydrogel bioink reinforcement for additive manufacturing: a focused review of emerging strategies, Adv. Mater. 32 (1) (2020), 1902026.
[26] H. He, D. Li, Z. Lin, L. Peng, J. Yang, M. Wu, D. Cheng, H. Pan, C. Ruan, Temperature-programmable and enzymatically solidifiable gelatin-based bioinks enable facile extrusion bioprinting, Biofabrication 12 (4) (2020), 049502.
[27] J.H.Y. Chung, S. Naficy, Z. Yue, R. Kapsa, A. Quigley, S.E. Moulton, G.G. Wallace, Bio-ink properties and printability for extrusion printing living cells, Biomater. Sci. 1 (7) (2013) 763–773.
[28] L. Li, C. Lu, L. Wang, M. Chen, J. White, X. Hao, K.M. Mclean, H. Chen, T. C. Hughes, Gelatin-based photocurable hydrogels for corneal wound repair, ACS Appl. Mater. Interfaces 10 (16) (2018) 13283–13292.
[29] B. Zhang, L. Gao, L. Ma, Y. Luo, H. Yang, Z. Cui, 3D bioprinting: a novel avenue for manufacturing tissues and organs, Engineering 5 (4) (2019) 777–794.
[30] C. Xu, G. Dai, Y. Hong, Recent advances in high-strength and elastic hydrogels for 3D printing in biomedical applications, Acta Biomater. 95 (2019) 50–59.
[31] H. Hong, Y.B. Seo, D.Y. Kim, J.S. Lee, Y.J. Lee, H. Lee, O. Ajiteru, M.T. Sultan, O. J. Lee, S.H. Kim, C.H. Park, Digital light processing 3D printed silk fibroin hydrogel for cartilage tissue engineering, Biomaterials 232 (2020) 119679.
[32] S.H. Kim, Y.K. Yeon, J.M. Lee, J.R. Chao, Y.J. Lee, Y.B. Seo, M.T. Sultan, O.J. Lee, J. S. Lee, S. Yoon, I. Hong, G. Khang, S.J. Lee, J.J. Yoo, C.H. Park, Precisely printable

and biocompatible silk fibroin bioink for digital light processing 3D printing, Nat. Commun. 9 (1) (2018) 1620.
[33] A.I. Van Den Bulcke, B. Bogdanov, N. De Rooze, E.H. Schacht, M. Cornelissen, H. Berghmans, Structural and rheological properties of methacrylamide modified gelatin hydrogels, Biomacromolecules 1 (1) (2000) 31–38.
[34] T. Wu, C. Cui, C. Fan, Z. Xu, Y. Liu, W. Liu, Tea eggs-inspired high-strength natural polymer hydrogels, Bioact. Mater. 6 (9) (2021) 2820–2828.
[35] C. Kilic Bektas, V. Hasirci, Mimicking corneal stroma using keratocyte-loaded photopolymerizable methacrylated gelatin hydrogels, J. Tissue Eng. Regen. Med. 12 (4) (2018) e1899–e1910.
[36] X. Dai, Y. Zhang, L. Gao, T. Bai, W. Wang, Y. Cui, W. Liu, A mechanically strong, highly stable, thermoplastic, and self-healable supramolecular polymer hydrogel, Adv. Mater. 27 (23) (2015) 3566–3571.
[37] H. Wang, Y. Wu, C. Cui, J. Yang, W. Liu, Antifouling super water absorbent supramolecular polymer hydrogel as an artificial vitreous body, Adv. Sci. 5 (11) (2018), 1800711.
[38] S. Liu, T. Jiang, R. Guo, C. Li, C. Lu, G. Yang, J. Nie, F. Wang, X. Yang, Z. Chen, Injectable and degradable PEG hydrogel with antibacterial performance for promoting wound healing, ACS Appl. Bio Mater. 4 (3) (2021) 2769–2780.
[39] S. Chameettachal, D. Prasad, Y. Parekh, S. Basu, V. Singh, K.K. Bokara, F. Pati, Prevention of corneal myofibroblastic differentiation in vitro using a biomimetic ECM hydrogel for corneal tissue regeneration, ACS Appl. Bio Mater. 4 (1) (2021) 533–544.
[40] M. Xeroudaki, M. Thangavelu, A. Lennikov, A. Ratnayake, J. Bisevac, G. Petrovski, P. Fagerholm, M. Rafat, N. Lagali, A porous collagen-based hydrogel and implantation method for corneal stromal regeneration and sustained local drug delivery, Sci. Rep. 10 (1) (2020), 16936.
[41] J. Zhu, Bioactive modification of poly(ethylene glycol) hydrogels for tissue engineering, Biomaterials 31 (17) (2010) 4639–4656.
[42] C. Liu, N. Morimoto, L. Jiang, S. Kawahara, T. Noritomi, H. Yokoyama, K. Mayumi, K. Ito, Tough hydrogels with rapid self-reinforcement, Science 372 (6546) (2021) 1078–1081.
[43] K. Rahali, G. Ben Messaoud, C. Kahn, L. Sanchez-Gonzalez, M. Kaci, F. Cleymand, S. Fleutot, M. Linder, S. Desobry, E. Arab-Tehrany, Synthesis and characterization of nanofunctionalized gelatin methacrylate hydrogels, Int. J. Mol. Sci. 18 (12) (2017) 2675.
[44] E. Shirzaei Sani, A. Kheirkhah, D. Rana, Z. Sun, W. Foulsham, A. Sheikhi, A. Khademhosseini, R. Dana, N. Annabi, Sutureless repair of corneal injuries using naturally derived bioadhesive hydrogels, Sci. Adv. 5 (3) (2019), eaav1281.
[45] X. Zhao, S. Li, X. Du, W. Li, Q. Wang, D. He, J. Yuan, Natural polymer-derived photocurable bioadhesive hydrogels for sutureless keratoplasty, Bioact. Mater. 8 (2021) 196–209.
[46] B. Wang, X. Xiao, Y. Zhang, L. Liao, High strength dual-crosslinked hydrogels with photo-switchable color changing behavior, Eur. Polym. J. 116 (2019) 545–553.
[47] M. Pircher, E. Götzinger, R. Leitgeb, A.F. Fercher, C.K. Hitzenberger, Measurement and imaging of water concentration in human cornea with differential absorption optical coherence tomography, Opt Express 11 (18) (2003) 2190–2197.
[48] S.M. Mccarty, S.L. Percival, Proteases and delayed wound healing, Adv. Wound Care 2 (8) (2013) 438–447.
[49] A. Sorkio, L. Koch, L. Koivusalo, A. Deiwick, S. Miettinen, B. Chichkov, H. Skottman, Human stem cell based corneal tissue mimicking structures using laser-assisted 3D bioprinting and functional bioinks, Biomaterials 171 (2018) 57–71.
[50] Z. Wu, X. Su, Y. Xu, B. Kong, W. Sun, S. Mi, Bioprinting three-dimensional cell-laden tissue constructs with controllable degradation, Sci. Rep. 6 (1) (2016), 24474.
[51] S. Sharifi, M.M. Islam, H. Sharifi, R. Islam, D. Koza, F. Reyes-Ortega, D. Alba-Molina, P.H. Nilsson, C.H. Dohlman, T.E. Mollnes, J. Chodosh, M. Gonzalez-Andrades, Tuning gelatin-based hydrogel towards bioadhesive ocular tissue engineering applications, Bioact. Mater. 6 (11) (2021) 3947–3961.
[52] D. Myung, K. Derr, P. Huie, J. Noolandi, K.P. Ta, C.N. Ta, Glucose permeability of human, bovine, and porcine corneas in vitro, Ophthalmic Res. 38 (3) (2006) 158–163.
[53] Y. Du, D.S. Roh, M.L. Funderburgh, M.M. Mann, K.G. Marra, J.P. Rubin, X. Li, J. L. Funderburgh, Adipose-derived stem cells differentiate to keratocytes in vitro, Mol. Vis. 16 (2010) 2680–2689.
[54] S.L. Wilson, I. Wimpenny, M. Ahearne, S. Rauz, A.J. El Haj, Y. Yang, Chemical and topographical effects on cell differentiation and matrix elasticity in a corneal stromal layer model, Adv. Funct. Mater. 22 (17) (2012) 3641–3649.
[55] B. Kong, L. Sun, R. Liu, Y. Chen, Y. Shang, H. Tan, Y. Zhao, L. Sun, Recombinant human collagen hydrogels with hierarchically ordered microstructures for corneal stroma regeneration, Chem. Eng. J. 428 (2022), 131012.
[56] X. Wang, Y. Yu, C. Yang, C. Shao, K. Shi, L. Shang, F. Ye, Y. Zhao, Microfluidic 3D printing responsive scaffolds with biomimetic enrichment channels for bone regeneration, Adv. Funct. Mater. 31 (40) (2021), 2105190.
[57] D.F. Duarte Campos, M. Rohde, M. Ross, P. Anvari, A. Blaeser, M. Vogt, C. Panfil, G.H.F. Yam, J.S. Mehta, H. Fischer, P. Walter, M. Fuest, Corneal bioprinting utilizing collagen-based bioinks and primary human keratocytes, J. Biomed. Mater. Res. 107 (9) (2019) 1945–1953.